Published in final edited form as:
*J Phys Chem C Nanomater Interfaces*. 2012 October 11; 116(40): 21563–21571. doi:10.1021/jp3072876.

# Large Fluorescence Enhancements of Fluorophore Ensembles with Multilayer Plasmonic Substrates: Comparison of Theory and Experimental Results

**Henryk Szmacinski**[*,†], **Ramachandram Badugu**[†], **Farhad Mahdavi**[‡], **Steve Blair**[‡], and **Joseph R. Lakowicz**[†]

[†]Center for Fluorescence Spectroscopy, Department of Biochemistry and Molecular Biology, University of Maryland Baltimore, 725 W. Lombard Street, Baltimore, Maryland 21201, United States

[‡]Department of Electrical and Computer Engineering, University of Utah, 50 S. Central Campus Drive, Room 3280, Salt Lake City, Utah 84112, United States

## Abstract

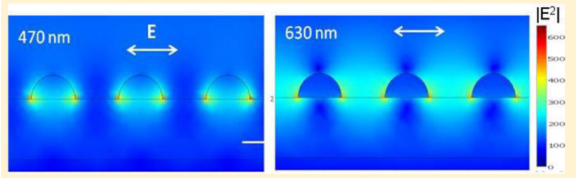


Multilayer substrates consisting of a glass slide, silver mirror, silica layer, and silver nanoparticles were fabricated using magnetron sputtering. This new geometry of substrates with backplane mirror and dielectric photonic cavity produced large average fluorescence enhancements up to 190-fold. Fluorescence enhancements of five fluorescent probes were measured over the broad spectral range from 470 to 800 nm. Fluorescent probes were streptavidin conjugates attached to the substrate surface through a layer of biotinylated bovine serum albumin. The protein layers represent a common surface modification for surface-based bioassays such as immunoassays or molecular diagnostic assays. We found that optimal enhancement is dependent on the thickness of the dielectric layer separating the silver mirror and the silver nanoparticles and on the spectral range. We performed numerical calculations for enhancement in both the excitation and emission using finite element method (FEM) the results of which were in qualitative agreement with the experimental results. The described method for fabrication multilayered substrates and the results obtained with protein layers demonstrate great potential for the design of simple and ultrasensitive fluorometric bioassays with large optical amplifications compared to the standard approaches of enzyme-based bioassays with dielectric surfaces.

## INTRODUCTION

Metal nanoparticles, in particular gold and silver, exhibit highly efficient interactions with visible and NIR light, resulting from the excitation of localized surface plasmon resonance (LSPR). LSPR induces large local field intensities that extend into and outside of the



[*]**Corresponding Author**: hszmacinski@umaryland.edu. .

The authors declare no competing financial interest.

nanoparticles. One of promising application of nanoparticle LSPR that is intensively explored by many groups is its use for the enhancement of fluorescence of organic (or aromatic) molecules. Organic fluorescent molecules are available across a broad spectral range from the UV to NIR and are widely used in biosciences. However, their applications are frequently limited because of insufficient brightness when ultrasensitive detection is required. The extensive research work to date pertaining to enhanced fluorescence using various metallic nanostructures has been recently reviewed;[1-3] thus, we limit our discussion to Ag nanoparticles deposited on planar surfaces. To date, the observed average fluorescence enhancements are similar for several fabrication methods, with none exceeding 50-fold. The most notable methods used for fluorescence enhancement on planar substrates include chemical deposition of silver island films on glass,[1-4] physical adsorption of Ag colloids,[1-3,5] and patterning methods based upon electron beam lithography.[6-10] Methods to produce precisely controlled sizes, shapes and interparticle separations such as electron beam lithography, nanoimprint lithography and nanosphere lithography have resulted in moderate fluorescence enhancements, typically less than 50-fold,[6-11] but an enhancement of 1340-fold was observed for single low quantum-yield molecules from lithographically fabricated bowtie nanoantenas.[12] The common understanding for effective enhancement has been to provide a strong overlap between the surface plasmon resonance band and excitation/ emission spectra of fluorophores. The key issues for plasmon enhanced fluorescence are the coupling of excitation light into an LSPR-fluorophore system (near-field) and decoupling of fluorescence emission for effective detection in the far-field. Ag nanoparticles deposited onto dielectric surfaces usually display optical density of 0.5 or less in the visible range,[4,5] which indicates that a large amount of excitation light is transmitted through the substrate and not effectively used for fluorophore excitation. Moreover, the emission is mostly isotropic, with a large fraction coupled into a dielectric substrate and not in the direction of the detector. To increase the excitation and emission efficiency, mirrors have been used underneath the metallic nanostructures. Direct deposition of Ag colloids onto an Au mirror resulted in average enhancement of 50-fold and hot spots enhancement up to 200-fold.[13] The use of a dielectric spacer layer between metallic nanoparticles and mirrors has been recently investigated in order to tune the plasmonic properties of particles and increase the field by coupling localized surface plasmons with surface plasmon polaritons.[14-22] Field intensity enhancements factors up to 5000-fold were predicted for a small separation between Ag nanoparticles and a planar mirror.[20,23] The position of the localized resonant plasmon modes of nanoparticles can be significantly tuned by changing the distance to metallic film or changing the refractive index of the dielectric spacer.[18,22] In other studies it was shown that localized surface plasmon resonance strongly interacts with waveguide modes of the dielectric layer[15,24] and can be used for efficient transfer of power from a fiber optic to a waveguide.[17]

Most of the experimental reports on fluorescence enhancements using planar plasmonic nanostructures have not clearly linked the observed enhancements with spectral characteristics of the plasmonic substrates or with theoretical calculations. This becomes more important if more complex plasmonic substrates are fabricated, where several physical mechanisms may contribute to the observed fluorescence enhancements. To obtain and reproduce the optimal enhancements, one needs to understand the contribution from each mechanism and properly implement layers of metals and dielectrics with specific thicknesses.

In this report we describe the composition of multilayered substrates that maximize the coupling of excitation and decoupling of emission that result in average fluorescence enhancements up to about 190-fold. Compared to our previous report[25] where we established conditions for fabrication process of planar plasmonic substrates, here we extend the evaluation of these substrates into far red and NIR spectral ranges. Moreover, numerical

calculations are performed using the finite-element method (FEM) that provide insights on understanding the excitation and emission contributions to the observed fluorescence enhancements and provide guidance for rational design of substrates with a dielectric photonic cavity.

## METHODS

### Substrate Fabrication

Glass slides (from VWR) were cleaned with "piranha solution" (35% $H_2O_2/H_2SO_4$, 1:3) overnight, rinsed with distilled deionized water and dried with nitrogen before performing vacuum deposition steps. (Caution: Piranha solution reacts strongly with organic compounds and should be handled with extreme caution. Do not store the solution in a closed container.) Metallic and dielectric layers were deposited using magnetron sputtering (AJA model ATC 1800-V). First, a 1.5 nm chromium layer was deposited on glass for adhesion of an Ag layer of 200 nm thickness. After deposition of Ag film, a silicon dioxide layer with thickness varying from 3 to 300 nm was added. A final thin layer of Ag of about 13 nm was deposited followed by thermal annealing in air at 180 °C for 1 h. Substrates with varied thicknesses of outer Ag layer and varied annealing temperatures were investigated previously.[25]

### Fluorescent Probe Immobilization

The surfaces of the substrates and reference glass slides were coated with biotinylated bovine serum albumin (BSA-Bt) using 100 μg/ mL solution in phosphate buffer with an incubation time of 1 h. This step formed a monolayer of BSA-Bt that facilitated the immobilization of streptavidin-dye conjugates (5 μg/mL). Streptavidin (SA) conjugated dyes are Alexa Fluors from Invitrogen (Carlsbad, CA), AF488-SA, AF647-SA, AF680-SA, and AF750-SA; and the infrared dye IRD800-SA from LiCOR (Lincoln, NE). Phosphate buffer (PB) pH 7.4 and biotinylated bovine serum albumin (BSA-Bt) were from Sigma-Aldrich. Ultrapure water (>18.0 MΩ) (Millipore Milli-Q gradient system) was used in the preparation of buffers and aqueous solutions. The schemes of multilayer substrates with immobilized dye-streptavidin conjugates are shown in Figure 1.

### Spectroscopic Measurements

Extinction spectra were measured with a Hewlett-Packard 8453 spectrophotometer relative to the bare glass. Reflectance spectra were acquired with a Varian Cary 100 Bio spectrophotometer equipped with an external specular reflection attachment with fixed angle of incidence of 12 degrees. For baseline correction, a reference aluminum mirror (reflectance accessory) was used. Scanningelectron microscopy (Hitachi SU-70) was used for surface morphology imaging. Fluorescence from surfaces was measured using an epi-fluorescence microscope (Axiovert 135TV, Zeiss, see Figure 1) with 10×, NA 0.30 objective (UPlanFl, Olympus). Excitation was provided using either a blue LED (Nichia NSPB500S) with peak wavelength at 470 nm or a red LED (Nichia NSPR510CS) at 630 nm, and the emission was observed through a band-pass filter of 535/50 nm (AF488-SA) and long pass filter above 655 nm (red dyes). An NIR reader Odyssey from LiCOR (Lincoln, NE) was used for NIR dyes at a laser excitation of 680 and 780 nm. Steady-state intensities were measured on the multilayer substrates and compared to the signal of the respective samples on bare glass. Fluorescence enhancement was determined as the intensity ratio of the fluorescence signal measured from the multilayer substrate over the signal from the respective reference sample on bare glass using identical experimental conditions. Time-resolved data were measured using a phase-modulation fluorometer (K2 from ISS, Champagne, IL). The LEDs were modulated by applying an RF driving signal from a Marconi model 2022A frequency synthesizer (from Marconi Instruments, Allendale, NJ) to the LED.[26]

### Numerical Calculations

Numerical calculations were based on the finite-element method (FEM) using COMSOL Multiphysics version 3.5a.[27,28] Two mechanisms of fluorescence enhancement caused by the multilayered substrates were considered: enhancement in the excitation and enhancement in the emission confined to the region where fluorescent probes are located. Thus we performed two set of calculations: (1) calculating the effect of coupling of excitation light into a multilayered substrate via average field intensity within a 10 nm layer above the surface and (2) calculating the emission enhancement of randomly distributed and randomly oriented dipoles (representing fluorophores) within a 10 nm layer above the Ag nanoparticles. Figure 2 shows the model used for the calculations. An array of semispherical Ag nanoparticles with radius of 60 nm and spacing 40 nm edge-to-edge was used to approximate the heterogeneous silver nanostructures as thick layer of water above the substrate surface. The calculated enhancements are relative to a system consisting of a 10 nm layer of silica above the reference glass substrate. We chose conditions that closely match our experimental parameters: layer thicknesses, excitation wavelengths, emission wavelengths, and respective refractive indices of environments. Silver dielectric properties were taken from ref 29.

## RESULTS AND DISCUSSION

### Optical Characterization of Substrate

Figure 3 shows the SEM image of Ag nanoparticles obtained after annealing the Ag film with mass thickness of 13 nm on silica coated glass. This Ag film was readily annealed, which formed nanostructures resulting in large fluorescence enhancements.[25] The Ag nanostructures can be considered as a collection of nanoparticles heterogeneous in size and shape. Using an imaged area of $2 \times 2\ \mu m^2$, the estimated filling factor is 24%, with about 11% of the area covered with circular particles of average diameter of 81 ± 26 nm and 13% with elongated particles of average size 77 nm × 132 nm.

The broad surface plasmon spectrum of Ag nanoparticles as shown in Figure 3a is a result of the plurality of sizes and shapes of the particles as well as the interactions between the particles. To facilitate the measurement of the extinction spectrum of the Ag nanoparticles alone, a silica-coated glass was used without the Ag mirror. Figure 3a also shows the calculated extinction spectrum for an Ag array of hemispherical particles with 60 nm diameter and interparticle spacing 40 nm determined from the calculated transmission of incident light ($E = \log(1/T)$). This Ag array resulted in a similar extinction spectrum to that of nanoparticles on the multilayer substrates and therefore was used for numerical calculations of excitation and emission enhancements. In Figure 3b are shown absorption and emission spectra of dyes used in experiment, which overlap with the plasmon spectrum of Ag nanoparticles.

We found that the reflectance spectra shown in Figure 4 were much more sensitive to changes in silica thickness than the extinction spectra. For small to moderate silica thicknesses of up to 75 nm, the spectra are similar in shape with progressively decreasing reflectance values with increasing silica thickness. When the silica thickness is increased above the 75 nm, the reflectance spectra are more complex, displaying well-defined minima and maxima specific to the particular silica thickness. The reflectance of a similar three-layer system (Ag mirror–silica-Ag thin film) was investigated experimentally and theoretically using a stratified model.[30] It was found that the reflectance minima depend critically on the Ag film absorption and the phase shift of the electromagnetic wave when double passing the dielectric layer. The optical path ($nd$, $n$ is the refractive index and $d$ is the physical thickness) in the silica layer does not follow the simple integer multiple ($m$) of $\lambda/2$

as is observed for Fabry-Perot type cavities consisting of two mirrors separated by distances of $nd = m(\lambda/2)$. When one of the cavity mirrors consists of Ag nanostructures, the resonance condition is modified by the phase shift of the localized surface plasmon of the Ag nanoparticles.[6,15] The incident light interacts with a photonic cavity formed by a silica layer with an Ag mirror on the bottom and Ag nanostructures on the top. The total phase shift upon reflection includes the roundtrip of the wave in the cavity, the phase shift due to reflection at the Ag mirror, and an additional phase shift due to the localized surface plasmon excitation of the Ag nanostructures. Reflectance properties of the substrates indicate that incident light can be highly reflected, almost to 100% as well as can be highly absorbed or transmitted (low reflectance of about 5%). The above measurements of UV-vis-NIR reflectance and extinction suggest a complex interaction of light with plasmonic structures coupled to a photonic cavity. Low reflectance values suggest an efficient coupling of incident light into a system. However, it is not obvious how the coupled excitation light is distributed within the system and whether it generates the desired near field intensity within the space where fluorophores are deposited on the surface of the substrate. Therefore, to better understand the fluorescence enhancement and to gain insights on rational design of the substrates, we used numerical calculations to determine the effect of variation in silica thickness of multilayered substrates on the excitation and emission enhancements for selected wavelengths. The important factor is the interplay between Ag surface plasmon resonance and resonance within a silica layer which can be constructive as well as destructive as indicated by the reflectance spectra.

## Calculation of Excitation Enhancement

For excitation enhancements, calculations were performed using a plane wave incident perpendicular to the substrate surface with excitation intensity $|E_{Y0}|^2$, where $Y$ (in plane of substrate surface) is the direction of the electric field. As a consequence of the Ag nanoparticles and multiple reflections within the dielectric layer, the total excitation intensity consists of intensities in three directions; $|E_Y|^2$, $|E_X|^2$ and $|E_Z|^2$. The excitation enhancement was calculated as the ratio of average electromagnetic power within the 10 nm volume above the surface of the substrate to that of bare glass with the same silica thicknesses. Figure 5 shows the excitation enhancements for selected incident wavelengths versus the thickness of the silica cavity. The choice of excitation wavelengths was consistent by the experimental setup as shown in Figure 3b by arrows. In addition, we included excitation at 530 nm that matches the extinction peak of Ag nanoparticles (Figure 3a). To illustrate the strong effect of combined mirror and AgNP on the excitation enhancement, the results for other substrates are also shown in Figure 5. For a substrate with the mirror and silica layer only, the excitation enhancement varies periodically with silica thickness as expected for a Fabry—Perot resonant cavity. For a substrate with AgNP, the excitation enhancements are weakly dependent on silica thickness (variation within 10–20%). The observed variations are mainly due to weak Fabry–Perot interferences within the silica cavity. These calculations indicate that the substrate with mirror, silica cavity, and AgNP provides the most efficient excitation enhancements. It is important to notice that the enhancement peak does not follow the wavelength dependence governed by Fabry-Perot interference. While the excitation enhancement is strongly dependent on silica thickness and wavelength, one should notice that the substrate with silica thickness of approximately 25-60 nm facilitates similar enhancements across a broadrange of excitation wavelengths. Using greater silica thicknesses above 150 nm, one can also obtain high excitation enhancement (second peak) which varies strongly with wavelength; therefore multiple spectrally distinct fluorophores may display very different enhancements or even quenching. Such strong wavelength dependence may be useful for construction of substrates for detection systems where some wavelengths need to be enhanced and other suppressed.

Owing to limited experimental data for greater silica thicknesses, no extensive calculations were performed above 200 nm.

The FEM calculations also provide the explanation how the coupled excitation light is distributed within the system, and whether it generates the desired near field intensity within the space where fluorophores are deposited on the surface of the substrate. Figure 6 shows distributions of excitation light within a 10 nm layer for two incident wavelengths of 470 and 630 nm and silica thickness of 50 nm. Calculations of distribution of excitation were performed for an Ag array of 40 nm particle diameter and 40 nm edge-to-edge spacing. The drastic effect of excitation wavelength on excitation enhancement suggests that the addition of the dielectric layer results in additional enhancement and shift of the surface plasmon resonance of particles toward longer wavelengths. By varying particle size and shape, and thickness of dielectric layer, one can calculate the optimal parameters for selected excitation wavelengths and particular fluorophores. The active area for fluorescence enhancement is defined by the spatial localization of the surface plasmon field. It is clear that the active area for enhanced intensity distribution for a wavelength of 630 nm spreads over the entire volume between the nanoparticles, thus efficiently exciting the randomly distributed fluorophores. Interestingly, the enhanced field intensity for 470 nm is confined to volumes close to the nanoparticle surfaces and also extends into the nanoparticles, so as a consequence is less efficient for excitation. The enhanced field which is confined inside the nanoparticles is dissipated into ohmic heating and not useful for fluorescence enhancement. The enhanced field in close proximity to the particles surface also is not useful for fluorescence enhancement because of potential adverse quenching effects in emission. Thus, the overall excitation enhancement for fluorescence on multilayered substrates originates from enhanced field intensity and its distribution into all polarization components.

## Calculation of Emission Enhancement

For emission enhancement calculations we assumed a random distribution of point dipoles (fluorophores) both in terms of the orientation of the transition dipole moments and in distances from the surface within a 10 nm conformal layer. The total number of dipoles was 81 in the volume of $100 \times 100 \times 10$ nm$^3$ with transition moments equally distributed over the X, Y, and Z direction (27 dipoles per direction). This translates to a dipole surface concentration of 1.35 pmol/cm$^2$ which correlates well with the estimated experimental maximal (complete streptavidin monolayer) concentration of about 6 pmol/cm$^2$. We found that a 2-fold increase of number of dipoles resulted in a minor increase in calculated emission enhancement of about 5%. While the emission spectra of fluorophores are broad, we considered four emitters with emissions at 550, 580, 680, 720, and 800 nm which mimic closely our selected fluorescent probes in the green, red, far red, and NIR, respectively (see Figure 3b and Table 1). The hypothetical emitter at 580 nm is related to an excitation wavelength of 530 nm, which is frequently used in biosensing. The power radiated by the ensemble of dipoles was monitored by integrating the Poynting's vector at a distance of500 nm in water above the surface within an 18° cone angle, which refract into air space with 24° cone angle. This is close to observed 17.5° using a 10× objective with NA 0.30; thus, the calculation directly includes the increase in collection efficiency due to increased directionality imposed by the multilayer structure.[24] Radiation from dipoles oriented along X and Y directions on the multilayer substrate were assumed equal because of the system symmetry. The enhancement factors were calculated relative to the reference system of the glass slide without any additional dielectric or metal layers. For the reference sample, only dipoles oriented in the Y direction were considered because of the photoselective excitation by the plane wave polarized in the Y direction.

The dipole emission enhancement factors were calculated relative to the reference system of the glass slide without any additional dielectric or metal layers, and therefore represent the

effective increase in radiative rate (i.e., radiative rate enhancement times collection efficiency enhancement). For the reference sample, only dipoles oriented in the Y direction were considered because of the photoselective excitation by the plane wave polarized in the Y direction. Results of FEM calculations for selected dipoles (emission wavelengths) are shown in Figure 7. The dependence of X dipole emission on silica thickness is similar to the excitation dependence (Figure 5a), for example, the enhancements are maximal at about 25 nm for excitation at 630 nm and for X-oriented emitter at 680 nm. However, the enhancement is quite different for the *Z*-oriented emitter; the greatest enhancement is observed for no silica layer, while some quenching (<1.0) or no enhancement (~1.0) is observed for most of the silica thicknesses. These numerical calculations are in agreement with recent theoretical work on interaction of rotating electric dipole emitters with nanocavities and finding that coupling is strongly orientation-dependent density of modes.[31]

## Calculated and Experimental Fluorescence Enhancements

Effects of the combined resonances within the silica layer and localized surface plasmons of the Ag nanoparticles on fluorescence were studied using several fluorophores that span the spectral range from blue to NIR. The spectral properties of the fluorophores are summarized in Table 1. All dyes are classified as bright fluorescent probes which display high extinction coefficients and quantum yields. The quantum yield of AF750 was determined relative to that of IRD800 of 0.15[32] and of AF680 relative to the AF647 of 0.33.[33] All values of the quantum yields are for probes in buffer solution. We acknowledge that the quantum yield of fluorophores when bound to surfaces can be different from that from solution and should be regarded as a comparative factor between selected fluorophores. We focused on using Alexa Fluors because of their good photostabilities and low self-quenching when used to label proteins.[34,35] The streptavidin conjugated dyes were immobilized on substrates that were precoated with BSA-Bt. The use of BSA-Bt and streptavidin conjugates allowed us to maintain identical geometrical conditions when using multiple fluorophores spanning a broad spectral range. The estimated average distance between fluorophores and the substrate surface is approximately 6–9 nm as defined by the dimensions of BSA and streptavidin.

Net fluorescence enhancements were estimated by the multiplication of excitation (factor enhancing absorption rate) and emission enhancements. Strictly, net fluorescence enhancement is calculated by the product of excitation rate enhancement, quantum yield enhancement, and collection efficiency enhancement,[36] but here we used the enhancement in effective radiative rate to avoid lengthy calculations while still providing good qualitative agreement with experiments.[28]

For direct comparison with experimental results, we considered average excitation enhancements as shown in Figure 5a and emission enhancements as shown in Figure 7a. We excluded dipoles in the Z direction because their contribution to overall enhanced fluorescence is very small and their correct inclusion would require including three orthogonal components for excitation and emission. For example, the calculated excitation intensity of Z component $|E_Z|^2$ (as scattered from incident Y direction) is 31.3, 13.4, 11.4, and 9.3% of total excitation intensity at 470, 630, 680, and 780 nm,respectively. The emission enhancement of $D_Z$ dipoles is noticeable only at the small silica thicknesses, below 25 nm. Since we used weak excitation intensities from LEDs, we also do not consider saturation conditions as we easily observed increases or decreases in fluorescence intensity upon changing LED driving current.

For the red and far red range there is an excellent agreement between calculated and observed enhancements as shown by the dependence on silica thickness in Figure 8 for Alexa Fluors 647 and 680. This means that the model used for the calculations adequately describes the electromagnetic properties of the substrates for this wavelength range. For

blue/green and NIR range we observed larger fluorescence enhancement than that obtained from calculations (Figure 9). Maximal calculated enhancement for 470/530 nm is 14-fold compared to that observed for AF488 of about 30-fold. Similarly, 81-fold is calculated for 780/800 nm and up to 190-fold is observed. These apparent quantitative discrepancies between calculated and observed values can be explained by the heterogeneous nature of the Ag nanoparticles, which support fluorescence enhancement over a much broader spectral range than the idealized Ag array used for the calculations. Furthermore, the disordered pattern of Ag particles may contribute to stronger field enhancement than calculated here using uniform spacing, as has been recently reported.[37] This is in agreement with the experimental extinction spectrum of Ag nanoparticles, which is broader than the calculated spectrum, and thus supports blue/ green enhancement as well as NIR. Even greater enhancement is anticipated for lower quantum yield fluorophores which might contribute to larger observed enhancements.[2,12,38] This might apply to IRD800 and AF750, which display lower quantum yields. We discuss this more below in the context of lifetime changes. Despite the complexity of the multilayered substrate, quantitative (red and far red) and qualitative agreement between calculated and experimental data indicates that the design of plasmonic materials for fluorescence enhancement can be well guided by numerical calculations. The important aspect of the calculations is that the two mechanisms for the observed fluorescence enhancements, excitation and emission, can be calculated separately, which allows for the design of an optimal system.

One might surmise that the magnitude of fluorescence enhancement includes a contribution from a larger number of fluorophores on the silver nanostructures compared to the planar glass. We assumed an array of semispherical particles with diameter 60 and 40 nm spacing (side-to-side), resulting in an increase of total surface area by about 28% compared to the flat surface. Neither numerical nor experimental data were corrected for this relatively small effect compared to observed large enhancements. Therefore, the observed large fluorescence enhancements are due primarily to surface-enhanced phenomena and not to the differences in the concentration of surface bound streptavdin-dye conjugates. In view of sensing applications, the increase of sensing active area is desirable for improved sensitivity.

## Fluorescence Lifetime

Lifetime measurements were performed using a frequency-domain fluorometer. Intensity decays were acquired for streptavidin conjugates when free in buffer solution, bound to reference glass surface, and when bound to the multilayered substrate surface. Typical intensitydecays are shown in Figure 10 for AF680-SA in the three environments. Analyses of the intensity decays were performed using a two-exponential decay model, and calculated average lifetimes are summarized in Table 1 for a silica thickness of 50 nm, where the greatest enhancements were observed. The detailed procedure of intensity decay analysis is described in ref 25. Average lifetimes less than about 50 ps are at the limits of our LED/ PMT-based fluorometer, therefore we provide the range of lifetime values for which similar fit values were obtained. It is evident that a dramatic decrease in average lifetime was observed for each of the fluorophores when immobilized on the multilayer substrate. Large decrease in the lifetime indicates that the radiative ($k_r$), nonradiative ($k_{nr}$), or both decay rates were modified by the presence of silver nanoparticles ($\tau = 1/(k_r + k_{nr})$).[4-6,12,22,36] The significant decrease in lifetime and simultaneous large fluorescence enhancement imply an increase of the radiative decay rate, which in consequence may lead to increased quantum efficiency of the fluorophore. However, accurate determination of the quantum efficiency in the total fluorescence enhancement requires calculations of both radiative and nonradiative decay rates ($Q = k_r/(k_r + k_{nr})$). It was reported that the increase in quantum efficiency can be up to 10-fold for a very weak dipole emitter with 1% quantum efficiency in free space with optimal distance between an emitter and silver particle surface of 2-15 nm.[36] Because we

were focused on relatively bright fluorophores we anticipate moderate increase in the average quantum efficiencies, likely for the lowest quantum yield of NIR dyes. The decrease in lifetime for AF488 (blue-green range) on the multilayer substrate is noticeably lower than for dyes at longer wavelengths, which is consistent with lower fluorescence enhancement and the expected distribution of the excitation (Figure 6).

## CONCLUSIONS

We have fabricated multilayered substrates and found optimal and unique dielectric thicknesses for large far-field fluorescence enhancement for probes across a wide spectral range. An average enhancement from about 31-fold in blue-green and up to 190-fold in the NIR range has been observed. Numerical calculations provided insights into the mechanisms of fluorescence enhancements through the near-field intensity effect on excitation and the effect of interaction of excited fluorophores with localized plasmons of the silver nanostructures, including increased emission collection due to the underlying silver mirror. Our results are important for understanding the fluorescence enhancing mechanisms, application of numerical calculations to real experimental conditions, and guiding a rational design of plasmonic substrates for biosensing applications in particular to biomolecular assays.

## Acknowledgments

This research was supported by NIH Grants R21CA147975, HG005090, HG002655, and 1S10RR26370. We also acknowledge the support of the Maryland NanoCenter and FabLabs. S.B. acknowledges partial support by NSF MRSEC Grant DMR 1121252.

## REFERENCES

(1). Stewart ME, Anderson CR, Thompson LB, Maria J, Grey SK, Rogers JK, Nuzzo RG. Chem. Rev. 2008; 108:494–521. [PubMed: 18229956]

(2). Lakowicz JR, Ray K, Chowdhury M, Szmacinski H, Fu Y, Zhang J, Nowaczyk K. Analyst. 2008; 133:1308–1346. [PubMed: 18810279]

(3). Fort E, Grésillon S. J. Phys. D: Appl. Phys. 2008; 41:1–31.

(4). Malicka J, Gryczynski I, Lakowicz JR. Anal. Chem. 2003; 75:4408–4414. [PubMed: 14632044]

(5). Lukomska J, Malicka J, Gryczynski I, Lakowicz JR. J. Fluoresc. 2004; 14:417–423. [PubMed: 15617384]

(6). Ditlbacher H, Felidij N, Krenn JR, Lamprecht B, Leitner A, Aussenegg FR. Appl. Phys. B: Laser Opt. 2001; 73:373–377.

(7). Pompa PP, Martiradonna L, Della Tore A, Della Sala F, Manna L, De Vittorio M, Calabi F, Cingolani R, Rinaldi R. Nat. Nanotechnol. 2006; 1:126–130. [PubMed: 18654164]

(8). Corrigan TD, Guo S, Phaneuf RJ, Szmacinski H. J. Fluoresc. 2005; 15:779–786.

(9). Szmacinski H, Lakowicz JR, Catchmark JM, Eid K, Anderson JP, Middendorf L. Appl. Spectrosc. 2008; 62:7–733.

(10). Yang B, Lu N, Qi D, Ma R, Wu Q, Hao J, Liu X, Mu Y, Reboud V, Kehagias N, Torres CMS, Yin FYC, Chen X, Chi L. Small. 2010; 6:1038–1043. [PubMed: 20394069]

(11). Chen Y, Munechika K, Ginger DS. Nano Lett. 2007; 7(3):690–696. [PubMed: 17315937]

(12). Kinkhabwala A, Yu Z, Fan S, Avlasevich Y, Müllen K, Moerner WE. Nat. Photonics. 2009; 3:654–657.

(13). Sørensen TJ, Laursen BW, Luchowski R, Shtoyko T, Akopova I, Gryczynski Z, Gryczynski I. Chem. Phys. Lett. 2009; 476:46–50. [PubMed: 20161182]

(14). Barnes WL. J. Mod. Opt. 1998; 45:661–699.

(15). Ameling R, Langguth L, Hentschel M, Mesch M, Braun PV, Giessen H. Appl. Phys. Lett. 2010; 97:253116.

(16). Soller JB, Hall DG. J. Opt. Soc. Am. B. 2002; 19:1195–1203.
(17). Maier S, Barclay PE, Johnson TJ, Friedman MD, Painter O. Appl. Phys. Lett. 2004; 84:3989–3992.
(18). Leveque G, Martin OJF. Opt. Lett. 2006; 31:2750–2752. [PubMed: 16936880]
(19). Cesario J, Gonzales MU, Cheylan S, Barnes WL, Enoch S, Quidant R. Opt. Express. 2007; 15:10533–10539. [PubMed: 19547406]
(20). Leveque G, Martin OJF. Opt. Express. 2006; 14:9971–9981. [PubMed: 19529391]
(21). Pillai S, Catchpole KR, Trupke T, Green MA. J. Appl. Phys. 2007; 101:093105.
(22). Mock JJ, Hill T, Degiron A, Zauscher S, Chilkoti A, Smith DR. Nano Lett. 2008; 8:2245–2252. [PubMed: 18590340]
(23). Yi M, Zhang D, Wang P, Jiao X, Blair S, Wen X, Fu Q, Lu Y, Ming H. Plasmonics. 2011; 6:515–519.
(24). McDaniel S, Blair S. Opt. Express. 2010; 18:17477–17483. [PubMed: 20721132]
(25). Szmacinski H, Badugu R, Lakowicz JR. J. Phys. Chem. C. 2010; 114:21142–21149.
(26). Sipior J, Carter GM, Lakowicz JR, Rao G. Rev. Sci. Instrum. 1996; 67:3795–3798.
(27). COMSOL. Multiphysics User's Guide, version 3.5. Comsol Inc; Burlington MA: 2006.
(28). Mahdavi F, Liu Y, Blair S. Plasmonics. 2007; 2:129–142.
(29). Weaver, JH.; Frederikse, PR. CRC Handbook of Chemistry and Physics. CRC Press; Boca Raton, FL: 2001.
(30). Leitner A, Zhao Z, Brunner H, Aussenegg FR, Wokaun A. Appl. Opt. 1993; 32:102–109. [PubMed: 20802667]
(31). Chizhik AI, Gregor I, Schleifenbaum F, Müller CB, Röling C, Meixner AJ, Enderlein. J. Phys. Rev. Lett. 2012; 108:163002.
(32). Waddel E, Wang Y, Stryjewski W, McWhorter S, Henry AC, Evans D, McCarley RB, Soper SA. Anal. Chem. 2000; 72:5907–5917. [PubMed: 11140756]
(33). Panchuk-Voloshina N, Haugland RP, Bishop-Stewart J, Bhalgat MK, Millard PJ, Mao F, Leung WY, Haugland RP. J. Histochem. Cytochem. 1999; 47:1179–1188. [PubMed: 10449539]
(34). Anderson GP, Nerurkar NL. J. Immunol. Methods. 2002; 271:17–24. [PubMed: 12445725]
(35). Berlier JE, Rothe A, Buller G, Bradford J, Gray DR, Filanoski BJ, Telford WG, Yue S, Liu J, Cheung CY, Chang W, Hirsh JD, Beechem JM, Haugland RP, Haugland RP. J. Histochem. Cytochem. 2003; 51:1699–1712. [PubMed: 14623938]
(36). Mahdavi F, Blair S. Plasmonics. 2010; 5:169–174.
(37). Nishijima Y, Rosa L, Joudkazis S. Opt. Express. 2012; 20(10):11466–11477. [PubMed: 22565766]
(38). Mertens H, Koendrink AF, Polman A. Phys. Rev. B. 2007; 76:115123.

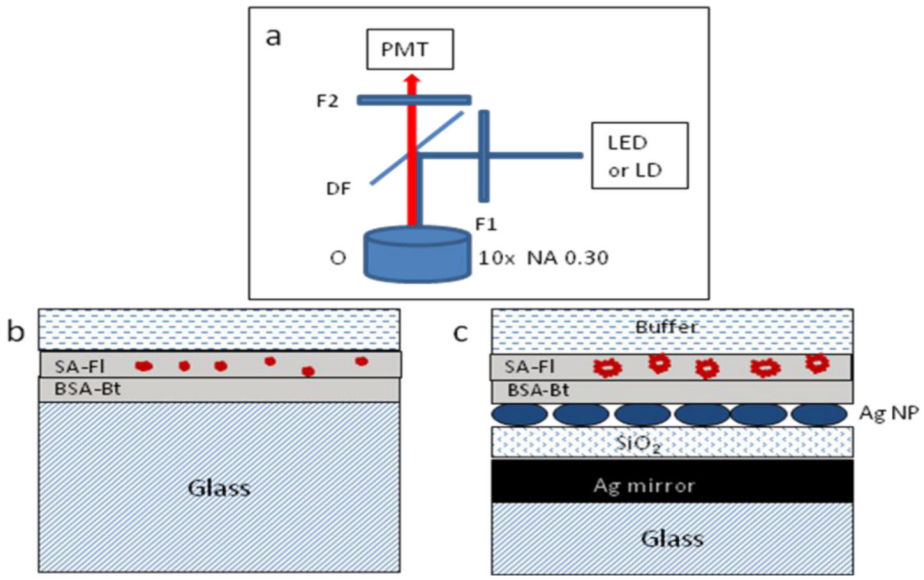


**Figure 1.**

Schemes of epifluorescence (a), geometrical configuration of reference sample (b), and multilayered substrate (c) with an immobilized layer of streptavidin-fluorophore (SA-Fl) on the layer of BSA-Bt. The specifics about the metal and dielectric layer thicknesses are within the text. The thicknesses in the figure are not to scale. The abbreviations of F1, F2, DF, and O are for the excitation, emission, dichroic filters, and microscope objective, respectively.

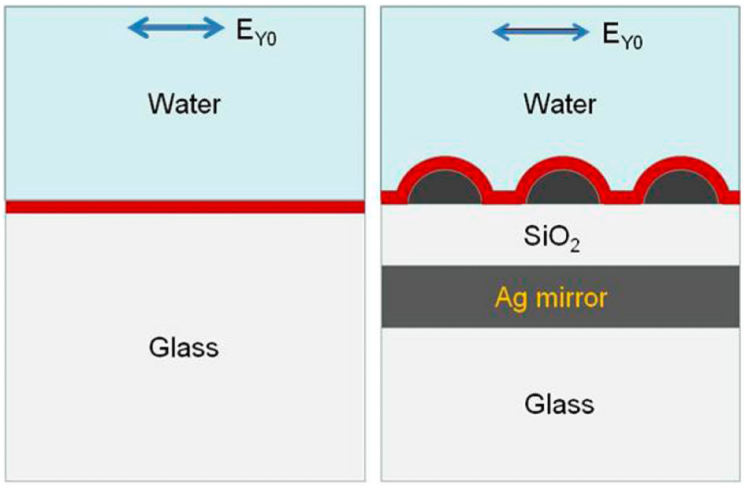


**Figure 2.**

Schemes of multilayer and reference models used for numerical calculations with parameters: Ag array of semispheres with diameter of 60 and 40 nm edge-to-edge spacing, Ag mirror with thickness of 200 nm, $SiO_2$ layer with variable thickness from 0 to 240 nm, and water thickness of 500 nm. The average excitation field intensity and radiation power of randomly distributed dipoles were performed using the entire volume of a layer of 10 nm above the silica (or glass) surface. The arrow shows the polarization of incident electrical field.

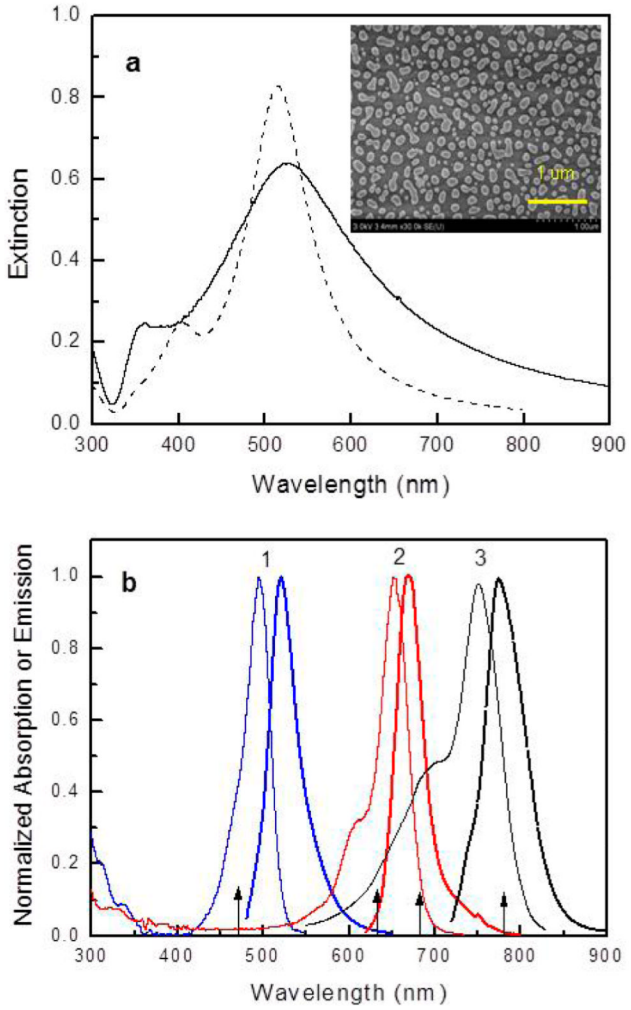


**Figure 3.**

(a) Extinction spectrum of Ag nanoparticles on silica coated glass (solid line) and the numerically calculated spectrum for Ag array of semispherical nanoparticles of 60 nm diameter and edge-to-edge spacing of 40 nm (dashed line). (Inset) SEM image of Ag nanoparticles. (b) Absorption (thin lines) and emission spectra (thick lines) of AF488-SA (1), AF647-SA (2), and AF750-SA (3). For clarity of figure, spectra of the AF680-SA and IRD800-SA are not included. They are about 30 nm red-shifted compared to AF647-SA and AF750-SA, respectively. Arrows indicate the experimental excitation wavelengths.

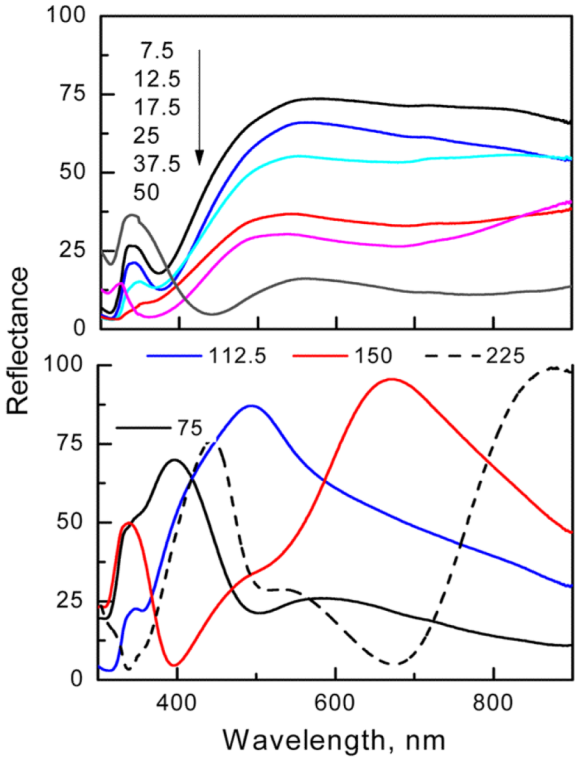


**Figure 4.**
Experimental reflectance spectra of multilayered substrates.

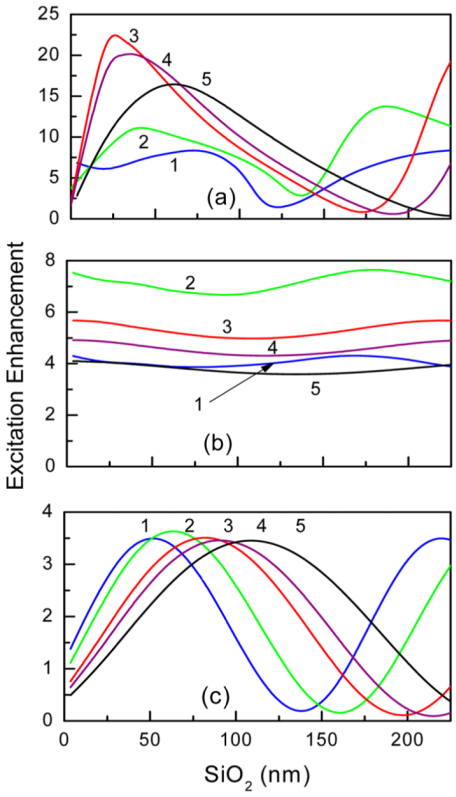


**Figure 5.**
Calculated average excitation enhancement within 10 nm layer above the surface for substrates with variation of silica cavity layer for selected incident wavelengths: (1) 470, (2) 530, (3) 630, (4) 680, and (5) 780 nm). (a) Substrate with mirror, silica layer, and AgNP array, (b) substrate with silica layer and AgNP array, and (c) substrate with mirror and silica layer.

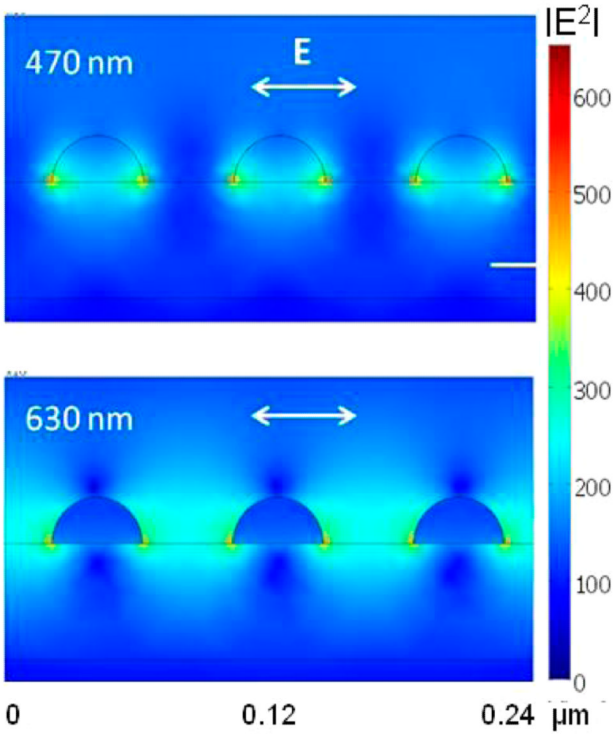


**Figure 6.**
Distribution of the excitation field intensity for 470 and 630 nm on a multilayer substrate. Calculations are for a Ag array with semispheres of 40 nm diameter and interparticle spacing of 40 nm (note that this array has smaller particles than used for other calculations and comparisons with experimental data). The polarization of incident field is in the plane of figure, from top.

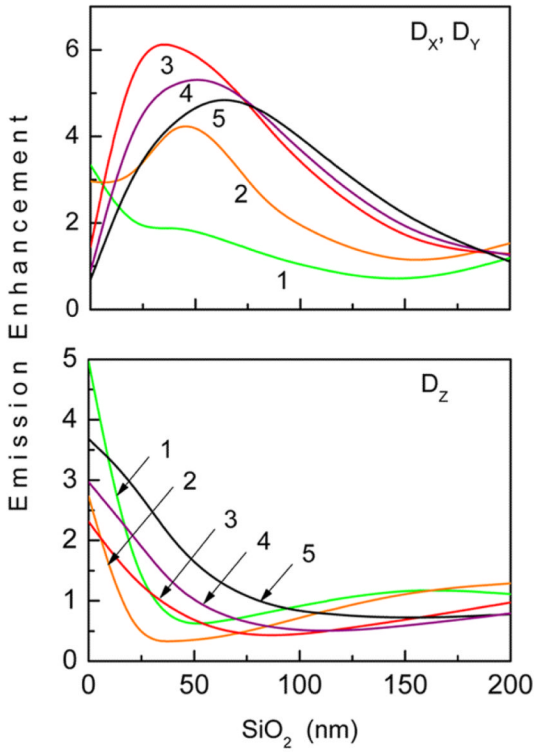


**Figure 7.**
Calculated average emission enhancement within 10 nm layer above the surface for substrates with variation of silica cavity layer for selected dipoles with emission wavelengths: (1) 550, (2) 580, (3) 680, (4) 720, and (5) 800 nm. Dipole transition moment is parallel (a) and perpendicular (b) to the surface. The measurement of radiation power is within a cone with 18 degrees.

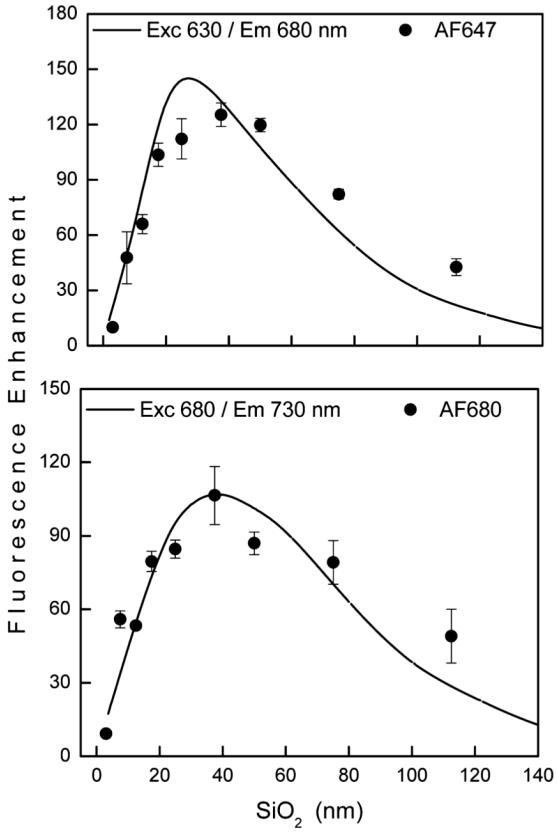


**Figure 8.**
Calculated (line) and experimental fluorescence enhancements (data points) for red (top) and far red (bottom) spectral range.

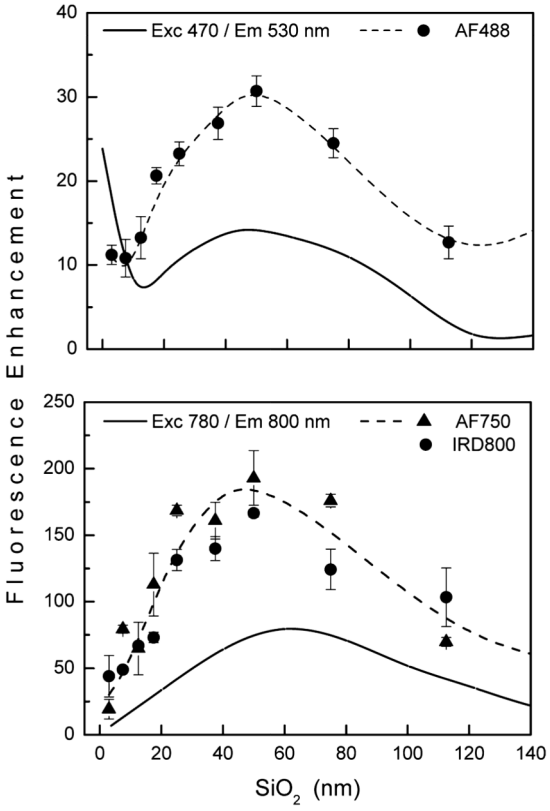


**Figure 9.**
Calculated (solid line) and experimental fluorescence enhancements (data points and dashed line) for blue/green (top) and NIR (bottom) spectral range. Dashed lines are drawn for visual guidance.

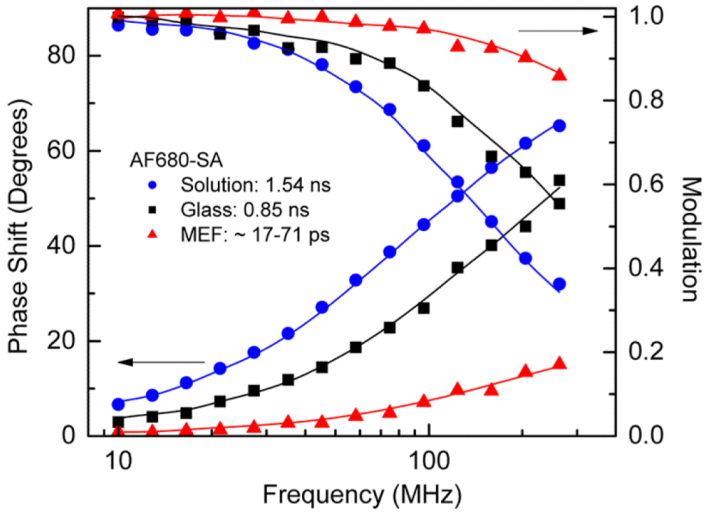


**Figure 10.**

Frequency-domain intensity decays of AF680-SA in three environments. The intensity decay (MEF) was measured for AF680-SA on a multilayered substrate with silica thickness of 50 nm. Lifetime data for other dyes are summarized in Table 1. The lines represent the best fit to the two-exponential decay model.

**Table 1**

**Spectral Properties of Streptavidin Conjugated Dyes in Solution and When Bound to the Multilayered Substrate**

| SA-dye conjugate | AF488 | AF647 | AF680 | AF750 | IRD800 |
|---|---|---|---|---|---|
| $\lambda_{exc}/\lambda_{ems}$ (nm) | 495/519 | 650/665 | 679/702 | 749/775 | 795/819 |
| ε ($M^{-1}$ $cm^{-1}$) | 71 000 | 239 000 | 184 000 | 240 000 | 207 000 |
| QY in solution | 0.4233 | 0.3333 | 0.30 | 0.12 | 0.1532 |
| $\langle\tau\rangle$ [a] in solution (ns) | 2.71 | 1.65 | 1.54 | 0.87 | 0.81 |
| $\langle\tau\rangle$ on glass (ns) | 1.06 | 0.77 | 0.85 | N/A | N/A |
| $\langle\tau\rangle$ on substrate (ns) | 0.28 | 0.023–0.078 | 0.017–0.071 | 0.033–0.072 | 0.015–0.055 |

[a] Amplitude weighted lifetime ($\langle\tau\rangle = \Sigma\alpha_i\tau_i$ where $\alpha_i$ is the pre-exponential factor and $\Sigma\alpha_i = 1$).

*J Phys Chem C Nanomater Interfaces*. Author manuscript; available in PMC 2013 October 23.